ARTICLE IN PRESS

Available online at www.sciencedirect.com
SCIENCE DIRECT®

ELSEVIER

Ocean Modelling xxx (2003) xxx–xxx

Ocean Modelling

www.elsevier.com/locate/omodol

A finite-element ocean model: principles and evaluation

Sergey Danilov *, Gennady Kivman, Jens Schröter

Alfred Wegener Institute for Polar and Marine Research, Postfach 12-01-61, 27515 Bremerhaven, Germany

Received 16 October 2002; received in revised form 13 December 2002; accepted 13 December 2002

Abstract

We describe a three-dimensional (3D) finite-element ocean model designed for investigating the large-scale ocean circulation on time scales from years to decades. The model solves the primitive equations in the dynamical part and the advection–diffusion equations for temperature and salinity in the thermodynamical part. The time-stepping is implicit. The 3D mesh is composed of tetrahedra and has a variable resolution. It is based on an unstructured 2D surface mesh and is stratified in the vertical direction. The model uses linear functions for horizontal velocity and tracers on tetrahedra, and for surface elevation on surface triangles. The vertical velocity field is elementwise constant. An important ingredient of the model is the Galerkin least-squares stabilization used to minimize effects of unresolved boundary layers and make the matrices to be inverted in time-stepping better conditioned. The model performance was tested in a 16-year simulation of the North Atlantic using a mesh covering the area between 7° and 80° N and providing variable horizontal resolution from 0.3° to 1.5°.

Keywords: Finite elements; Ocean modelling

1. Introduction

The idea of using unstructured grids for modelling ocean dynamics sounds very attractive given high complexity of the ocean geometry. Fine topographic features like narrow straits, steep continental slopes, islands, etc. are of crucial importance and may control the circulation on large spatial scales while they can hardly be resolved with an affordable homogeneous spatial resolution. The finite-element method (FEM) offers a traceable tool to tackle this problem.

* Corresponding author.
E-mail addresses: sdanilov@awi-bremerhaven.de (S. Danilov), gkivman@awi-bremerhaven.de (G. Kivman), jschroeter@awi-bremerhaven.de (J. Schröter).

1463-5003/03/$ - see front matter
doi:10.1016/S1463-5003(02)00063-X

Most extensively, the FEM is used in modelling barotropic tides and wind-driven ocean circulation (Walters and Werner, 1989; Le Provost and Vincent, 1991; Wunsch et al., 1997; Myers and Weaver, 1995), and some tests proved that results obtained with the FEM were favorable in comparison to those obtained with more traditional finite-difference methods (FDMs) (see Dumas et al., 1982). Attractiveness of the FEM for modelling ocean dynamics was demonstrated more at the dawn of the age of ocean circulation modelling by Fix (1975). Such nice properties of the FEM as conservation of energy that is common for all variational methods of solving differential equations, natural treatment of boundary conditions, and flexibility of triangulation were complemented with availability of supercomputers. The high ratio of inter-element to intra-element calculations makes the FEM well suited to parallel computing. Having these in mind Le Provost (1986) suggested this approach as an interesting alternative to the FDM commonly used in ocean modelling.

However, not much changed since that time. Few applications of the FEM to steady-state ocean inverse problems (Brasseur, 1991; Schlichtholz and Houssais, 1999; Dobrindt and Schröter, 2002a,b; Nechaev et al., 2003) appeared. Some existing two-dimensional (2D) FE shallow water tide models have been generalized by accounting for the dependence on the vertical coordinates with the FDM (Westerink et al., 1992; Lynch and Naimie, 1993) and by including heat and salt advection (Lynch et al., 1996). But they are exclusively used in modelling the coastal dynamics for relatively short time periods (up to few months). A model developed by Iakovlev (1996) relies on three-dimensional (3D) FEs but essentially uses a structured horizontal mesh that allows one to retain conservation properties of the FEM and to avoid algorithmic complexity encountered while using unstructured meshes. However, this approach does not employ the whole potential of the FEM such as capability to follow nicely complex boundaries and to provide finer resolution in frontal zones and regions of special interest.

Despite remarkable achievements gained with the FEM in simulating coastal and tidal dynamics, ocean general circulation models (OGCMs) used in climatic studies still almost exclusively rely on the FDM. The only exception is the spectral element ocean model (SEOM) (Iskandarani et al., 1995). In a recent review of the OGCMs, Griffies et al. (2001) pointed out that in addition to algorithmic complexity there are two general problems one would encounter in using unstructured grids. First, it is difficult to represent the geostrophic balance on the unstructured grid. Second, any change in grid spacing gives rise to unphysical wave scattering that is not dangerous for steady state engineering problems or for ocean circulation problems at relatively short integration time (as is the case for tide and coastal models) but might become of crucial importance for modelling large-scale ocean circulation.

With this regard, it is worth emphasizing the basic distinction between the FDM and FEM. Namely, using the former one redefines the differential model operator while the latter allows to preserve the operator by changing the space where the solution is searched for. With special care in choosing the functional spaces for unknown model variables it is possible to resolve the first problem (Le Roux et al., 1998). The second problem can be mainly addressed to OGCMs employing curvilinear coordinates (POM, HOPE, etc.) rather than to the FEM. The FEM is conservative and preserves almost all properties of the original differential operator to be inverted. Of sure, with the spatial resolution varying very sharply or with elements having bad discretization properties (for example, triangles containing small angles) the set of algebraic equations to be

solved becomes extremely ill-conditioned. However it is not a problem of the FEM itself and it should be solved at the step of the mesh generation.

Here, we present the first 3D FE primitive equations ocean circulation model based on an unstructured horizontal mesh. It is developed for studies of the large scale ocean circulation at time scales from months to decades. Unlike the SEOM where a relatively new approach of spectral elements (Patera, 1984) is utilized we use a more traditional formulation of the FEM. The basic difference between them is as follows. With the FEM, one uses low order polynomials as basis functions defined on a relatively high number of basic elements. It is opposed to the spectral element method where the polynomials are of much higher order while the partitioning of the computational domain is much coarser.

The basic elements in our model are tetrahedra. The mesh is stratified in the vertical and is unstructured in the horizontal directions. This choice allows the coast lines and the bottom topography to be followed very precisely and notably simplifies the vertical integration for computing the hydrostatic pressure. Horizontal velocity, temperature and salinity are chosen to belong to the space of linear functions defined on tetrahedra. The sea surface height belongs to the space of linear functions on surface triangles, and vertical velocity is elementwise constant.

The model has grown from the diagnostic FE model by Nechaev et al. (2003) and borrows its choice for functional spaces to represent the model fields. It differs, however, in many other important respects. First, it is designed for time-stepping mode, although it allows for stationary inversion as an option. Second, it uses Galerkin least-squares (GLS) stabilization (Hughes et al., 1989) modified for transient problems which ensures stable performance with time steps up to 12 h. Finally, it pays special attention to the accuracy of volume conservation.

Unlike the FD method exclusively used in ocean modelling for more than three decades, the history of FE applications is much more shorter and numerical problems one encounters when using the FEM are much less studied. The FEM was initially designed and is mainly applied to steady-state elliptic boundary-value problems. The primitive equations commonly used to describe the large-scale ocean circulation contain elliptic-type problems, but also require to solve the first-order continuity and hydrostatic equations. Treating them with 3D FEs on large unstructured meshes is not straightforward and we discuss several feasible approaches. Although some of them proved impractical, we believe that our experience might be useful for future development in the FE ocean modelling. Another problem comes from the fact that given low order polynomials on elements one cannot use biharmonic viscosity and diffusion to stabilize the momentum and tracer equations, as is becoming common with current eddy-permitting or eddy-resolving FD models. A set of residual-free stabilization techniques is known for FEM (see, e.g., Hughes et al., 1989; Hughes, 1995; Franca and Russo, 1996; Codina and Soto, 1997), which stabilize the equations without introducing excessive dissipation. The implementation of stabilization in primitive equations is also discussed in some detail below.

Sections 2 and 3 describe the model equations and discretization respectively, and Section 4 introduces stabilization. We also address the volume conservation there. The results of 16-year simulation of circulation in the Northern Atlantic are presented in Section 5. Section 6 concludes, and Appendices A and B contain analysis of dispersion properties of stabilized FE advection–diffusion equation and details of barotropic–baroclinic splitting.

2. Model equations

The governing equations of the model describe the thermo-hydrodynamics of a thin stratified layer of sea water on spherical rotating Earth under hydrostatic, Boussinesq and traditional approximation for the Coriolis terms. To avoid simultaneous treatment of non-linear dynamics and thermodynamics of the ocean we split the system of governing equations into two sub-problems and solve them separately.

The dynamical part of the model solves the momentum evolution equation under the integral continuity constraint:

$$\partial_t \mathbf{u} + f(\mathbf{k}\times\mathbf{u}) + g\nabla\zeta - \nabla\cdot A_l\nabla\mathbf{u} - \partial_z A_v \partial_z \mathbf{u} = -\frac{1}{\rho_0}\nabla p + \mathbf{F}_u, \tag{1}$$

$$\partial_t \zeta + \nabla\cdot\int_{z=-H}^{z=\zeta} \mathbf{u}\,dz = 0, \tag{2}$$

$$\partial_z p = -g\rho, \tag{3}$$

where $(\mathbf{u}, w) \equiv (u, v, w)$ is the velocity vector in the spherical coordinate system (λ, θ, z), ρ_0, ρ are the mean sea water density and the deviations from that mean respectively, ζ is the sea surface elevation, p is the baroclinic pressure anomaly computed from the level $z = 0$, $f = f(\theta)$ is the Coriolis parameter, A_l, A_v are the lateral and vertical momentum diffusion coefficients, $\mathbf{k}$ is the vertical unit vector, and g is the gravitational acceleration. The term $\mathbf{F}_u = (\mathbf{u}\nabla + w\partial_z)\mathbf{u}$ represents non-linear advection in the momentum equation. The term with time derivative in (2) is omitted in the rigid-lid approximation which filters out fast gravity waves. In this approximation the vertical velocity would satisfy zero boundary condition at $z = 0$. Although the rigid-lid approximation is the main option in the model, we will describe both the free-surface and rigid-lid versions. The upper limit of integration in (2) is set to 0, which is good approximation everywhere except for coastal regions.

The dynamical part of the model considers the density variation ρ to be known. Eqs. (1)–(3) are solved in a region Ω limited by four physically different types of boundaries $\partial\Omega = \bigcup_{i=1}^{4} \Gamma_i$, where $\Gamma_1 : \{z = 0\}$ stands for the ocean surface, $\Gamma_2 : \{z = -H(\lambda, \theta)\}$ is the bottom of the ocean, Γ_3 represents the lateral vertical rigid walls of the domain and Γ_4 denotes the lateral vertical *open* boundaries. The set of boundary conditions used with the dynamical part of the model includes the condition of the momentum flux continuity on the ocean surface, the bottom-drag condition on the bottom, no-slip boundary conditions on the vertical walls and the open-boundary condition:

$$A_v\partial_z\mathbf{u} = \boldsymbol{\tau},\ p = 0 \quad \text{on } \Gamma_1, \tag{4}$$

$$A_v\partial_z\mathbf{u} + A_l(\nabla\cdot H\nabla)\mathbf{u} = C_g\mathbf{u}|\mathbf{u}| \quad \text{on } \Gamma_2, \tag{5}$$

$$\mathbf{u} = 0 \quad \text{on } \Gamma_3, \qquad \mathbf{u} = \mathbf{v}_{OB}, \quad \text{on } \Gamma_4, \tag{6}$$

where $\boldsymbol{\tau}$ is the vector of tangent wind stresses, the friction coefficient $C_g = 0.0025$, and $\mathbf{v}_{OB}$ is a given velocity field at the open boundary.

In *the thermodynamical part* of the model we consequently solve the continuity equation for the vertical velocity w, tracer evolution equations for the potential temperature T and the salinity S of sea water, and compute density via the equation of state:

$$\partial_z w = -\nabla \cdot \mathbf{u}, \tag{7}$$

$$\partial_t C^m + \nabla \cdot (\mathbf{u} C^m) + \partial_z (w C^m) - \nabla \cdot K_l^m \nabla C^m - \partial_z K_v^m \partial_z C^m = 0, \tag{8}$$

$$\rho - \varrho(T, S, p) = 0. \tag{9}$$

Here $C^1 \equiv T$, $C^2 \equiv S$, K_l^m, K_v^m are the lateral and vertical diffusion coefficients for the mth tracer.

The vertical velocity is integrated from the ocean surface with the kinematic boundary condition:

$$w = \partial_t \zeta \quad \text{on } \Gamma_1$$

or

$$w = 0 \quad \text{on } \Gamma_1 \tag{10}$$

in the rigid-lid mode. It also obeys the second boundary condition at the bottom:

$$w = -\nabla H \cdot \mathbf{u} \quad \text{on } \Gamma_2 \tag{11}$$

implicit in (2). Tracer evolution equations (8) satisfy the following boundary conditions on the surface and solid boundaries:

$$K_v^m \partial_z C^m = -q^m \text{ or } C^m = C_0^m \quad \text{on } \Gamma_1, \tag{12}$$

$$(\nabla C^m, \partial_z C^m) \cdot \mathbf{n}_3 = 0 \quad \text{on } \Gamma_2 \cup \Gamma_3, \tag{13}$$

where q^m and C_0^m are the surface fluxes and surface values of the mth tracer, $\mathbf{n}_3$ is the 3D unit vector normal to the respective surface.

The boundary conditions at open boundaries are extensively discussed in the literature (see, e.g., the recent paper by Marchesiello et al. (2001)). No choice of open boundary conditions is mathematically consistent, and one is usually guided by the principle that the numerical solution be stable and realistic with respect to observational data. For the purpose of testing the model we set $\mathbf{v}_{OB} = 0$ in (6) and use

$$(\nabla C^m, \partial_z C^m) \cdot \mathbf{n}_3 = 0 \quad \text{on } \Gamma_4 \tag{14}$$

for tracers, realizing that the solution may depart from the desired one in some vicinity of the open boundaries. There are no principal difficulties in equipping the model with more "realistic" treatment of open boundary conditions.

3. Space and time discretization

3.1. Spatial discretization

A necessary prerequisite of any FE model is the choice of spatial discretization and definition of discrete functional spaces. We use tetrahedral elements obtained by constructing the surface triangular mesh, cutting the vertical prisms built on surface triangles by a set of horizontal (in upper

layers) and terrain-following (in deep layers) surfaces, and then cutting the elementary prisms into tetrahedra. This provides high flexibility for representation of irregular topography and local mesh refinement.

In choosing functional spaces we were guided by two principles. First, a major feature of the ocean dynamics is the dominance of the geostrophic balance in the ocean interior. Not every choice of velocity–pressure pairs of FE functional spaces is suitable for reproducing this balance. The problem was thoroughly examined by Le Roux et al. (1998) who concluded that the space of piecewise linear basis functions X for velocity and pressure is one of the most convenient from this point of view. Second, the piecewise linear basis functions require only nodal values of respective fields and thus provide compact storage for the fields and, more importantly, the matrices associated with equations. The latter factor becomes very restrictive as the size of the problem grows. Given all that, we choose linear basis functions for the horizontal velocity, sea surface height, hydrostatic pressure and tracers. The vertical velocity will be addressed separately.

However, these basis functions are not twice differentiable and we need to reformulate the problem (1)–(6) and (7)–(14) in the weak sense. Multiplying (1) and (2) respectively by an arbitrary vector field $\tilde{\mathbf{u}}$ and a scalar function $\tilde{\zeta}$ that does not depend on z, by making use of Green's formula and boundary conditions (4)–(6) we arrive at the equalities

$$\int_\Omega [(\partial_t \mathbf{u} + f[\mathbf{k}\times\mathbf{u}] + g\nabla\zeta)\cdot\tilde{\mathbf{u}} + A_v \partial_z \mathbf{u}\cdot\partial_z\tilde{\mathbf{u}} + A_l \nabla\mathbf{u}\cdot\nabla\tilde{\mathbf{u}}]\,d\Omega$$
$$= \int_{\Gamma_1} \boldsymbol{\tau}\cdot\tilde{\mathbf{u}}\,d\Gamma_1 - \int_{\Gamma_2} C_g|\mathbf{u}|\mathbf{u}\cdot\tilde{\mathbf{u}}\,d\Gamma_2 - \int_\Omega [(\mathbf{u}\cdot\nabla + w\partial_z)\mathbf{u}]\cdot\tilde{\mathbf{u}}\,d\Omega - \int_\Omega \frac{1}{\rho_0}\tilde{\mathbf{u}}\cdot\nabla p\,d\Omega, \tag{15}$$

$$\int_{\Gamma_1} \partial_t\zeta\tilde{\zeta}\,d\Gamma_1 - \int_\Omega \mathbf{u}\cdot\nabla\tilde{\zeta}\,d\Omega = -\int_{\Gamma_4} \mathbf{v}_{OB}\cdot\mathbf{n}_3\tilde{\zeta}\,d\Gamma_4 \tag{16}$$

to be fulfilled by the solution to the original problem (1)–(6) if $\tilde{\mathbf{u}} = 0$ on $\Gamma_3 \cup \Gamma_4$ where Dirichlet boundary conditions for the velocity field $\mathbf{u}$ are imposed. The last term in (16) is equal to zero if the open boundary is replaced by a rigid wall, and the first term should be omitted in the rigid lid approximation. After partitioning of the model domain onto tetrahedrons, we express model variables $\mathbf{u}$ and ζ as linear combinations of 3D and 2D piecewise linear basis functions X_k and S_k corresponding to the partitioning,

$$\mathbf{u} = \sum_{k=1}^{N_{3D}} \mathbf{u}_k X_k, \qquad \zeta = \sum_{k=1}^{N_{2D}} \zeta_k S_k. \tag{17}$$

The kth basis function is equal to 1 at the kth node and linearly vanishes to 0 within tetrahedrons (triangles) containing this node. Replacing the test functions $\tilde{\mathbf{u}}$ and $\tilde{\zeta}$ in (15) and (16) with X_i and S_i, we obtain the so-called Galerkin equations for $\mathbf{u}_k$ and ζ_k which represent nodal values of the velocities and sea surface height. Here N_{3D} and N_{2D} are the total amounts of 3D and 2D (surface) mesh nodes, respectively.

Before proceeding to the tracer equations, we will discuss discretization of the hydrostatic equation (3) and the vertical velocity (continuity) equation (7). Both require solving the first-order differential equation with respect to the vertical coordinate z. Unlike the FDM, this step is not trivial in the FEM, as the FEM always couples a given node with its neighbours thus leading to a matrix problem involving all nodes. Since the FEM in the space of linear functions is analogous to

approximating the derivatives with central differences, it couples together either the odd or even vertical levels while these two chains are linked only due to the boundary condition at the surface. As such, the corresponding stiffness matrix is generally ill-conditioned and leads to solutions with spurious level-to-level oscillations. To avoid them, the following strategy was adopted for the pressure p.

After computing T and S, we compute nodal values of ρ via the equation of state. Then we recover the nodal values of pressure from the hydrostatic equation considered in the FD sense. After obtaining nodal values p_k, the pressure is treated analogously to (17) as

$$p = \sum_{k=1}^{N_{3D}} p_k X_k \tag{18}$$

to compute the last term on the RHS of (15) in the FEM sense. Another scheme was also tested. Namely, we interpolated ρ linearly between the nodes and solved the second-order equation for p:

$$\partial^2_{zz} p = -g\,\partial_z \rho, \tag{19}$$

with the FEM in the space of piecewise linear functions (solving includes rewriting (19) in the weak sense, integrating by parts and obtaining a linear system of equations on p_k). In addition to the boundary condition at the surface $p = 0$ it needs the second boundary condition either at the surface or at the bottom. It could be taken from the hydrostatic equation. Our experience with this scheme of calculating p shows that due to finite accuracy of solution for p_k the pressure gradient is too noisy to be used as forcing in the momentum equation. So, the current default option consists in discretizing the hydrostatic equation by the FDM.

A procedure of this kind cannot be implemented for computing w for two reasons. First, a scheme of computing w must be consistent with (16) in order to fulfill boundary conditions (10) and (11). Second, the 2D divergence of the piecewise linear horizontal velocity $\mathbf{u}$ is not defined at nodes but at elements and thus we can treat the continuity equation (7) only in the weak sense. To go around solving the first-order problem for w, we introduce the vertical velocity potential Φ so that $w = \partial_z \Phi$. If $\Phi \in X$, then (7) can be reformulated with use of (10) and (11) as

$$\int_\Omega \partial_z \Phi\, \partial_z \tilde{\Phi}\, \mathrm{d}\Omega = -\int_\Omega \mathbf{u} \cdot \nabla \tilde{\Phi}\, \mathrm{d}\Omega + \int_{\Gamma_4} \mathbf{v}_{\mathrm{OB}} \cdot \mathbf{n}_3 \tilde{\Phi}\, \mathrm{d}\Gamma_4, \tag{20}$$

which should be held for any $\tilde{\Phi} \in X$. After computing Φ we obtain w as an elementwise constant function. With this scheme of treating the continuity equation we cannot guarantee the volume conservation within each tetrahedron. However, the volume is conserved locally within a cluster of elements surrounding each node (weighted with the test-function defined at this node), and globally. To see the latter take $\tilde{\Phi} = \mathrm{const}$, which would imply volume integration of the original continuity equation. Realizing that the surface integral is zero as there is no net volume flux through the open boundaries, we conclude that all terms in (20) become zero, or that the total volume is conserved.

Since both boundary conditions in this scheme are of the Neumann type, the RHS of (20) must satisfy the solvability condition: it must be zero for test functions that do not depend on the vertical coordinate, $\tilde{\Phi} = \tilde{\Phi}(\lambda, \theta)$. The latter is guaranteed up to numerical errors as the horizontal velocity field satisfies (16).

It is worth noting that another scheme for computing w is implemented in other FE models. It was found that integrating the continuity equation over z to calculate w resulted in accumulation of errors, for the reasons explained above. To prevent this undesired feature, Lynch and Naimie (1993) suggested to solve the second-order equation obtained by differentiating (7) with respect to z

$$\int_\Omega \partial_z w \partial_z \tilde{\Phi} \, \mathrm{d}\Omega = -\int_\Omega (\nabla \cdot \mathbf{u}) \partial_z \tilde{\Phi} \, \mathrm{d}\Omega, \tag{21}$$

with two Dirichlet boundary conditions (10) and (11). The fundamental difference between (20) and (21) is that the latter equation must be satisfied not for all test functions $\tilde{\Phi}$ but only for those vanishing at Γ_1 and Γ_2. Consequently, the global volume conservation is broken. Muccino et al. (1997) proposed to treat the continuity equation and boundary conditions (10) and (11) in the least-square sense and concluded that this approach outperformed that of Lynch and Naimie (1993). Though the least-square scheme has shown to provide less deterioration in volume conservation, the problem is still present. That was the reason why we did not proceed in either way.

The weak formulation for the tracer transport equations is grossly similar to that for the momentum equation. The advection of tracer fields (represented by linear combinations of piecewise linear basis functions) is computed using piecewise linear horizontal velocities and elementwise constant vertical velocities. We write down the weak formulation for the temperature equation only:

$$\int_\Omega (\partial_t T \widetilde{T} + (\mathbf{u} \cdot \nabla + w \partial_z) T \widetilde{T} + K_\mathrm{l} \nabla T \cdot \nabla \widetilde{T} + K_\mathrm{v} \partial_z T \partial_z \widetilde{T}) \, \mathrm{d}\Omega = -\int_{\Gamma_1} q \widetilde{T} \, \mathrm{d}\Gamma_1, \tag{22}$$

where q is the diffusive flux of tracer at the surface (negative flux would imply heating). The weak formulation for salinity or any other tracer would look similar to that for the temperature.

In the ocean FD modelling community much attention is paid to the choice of the advection scheme (see, e.g., Gerdes et al., 1991; Webb et al., 1998; Hecht et al., 2000). Many of current implementations use upwind-type corrections to the standard central differences which otherwise are too dispersive on small scales and result in oscillations in tracer fields if the diffusion is not sufficiently strong. The higher-order advection schemes exhibit reduced dispersion and biharmonic-type numerical diffusion. In this respect we would like to reiterate that the FE operator is exact, and it is the space of functions and partition onto elements which influence the solution. In Appendix A we present analysis of dispersion properties of FE disretized advection–diffusion equation and show them to be superior over central differences (FD) given one-dimensional (1D) problem and equidistant grid.

3.2. Time stepping

Several general remarks concerning time-stepping for FE discretized equations are worth noting. Due to a non-diagonal shape of the mass matrix formed by L_2 products of the basis functions, time stepping involves numerical matrix inversion. No solver can do it precisely, so differentiation of time-evolving FE fields is unsafe. The numerical noise due to finite accuracy of the solver may accumulate in time if differential operators are computed at the preceding time step. Therefore, the (most dangerous) second-order operators in (15) and (22) (viscosity and

diffusion respectively) should be treated implicitly (or at least, semi-implicitly). They lead to symmetrical contributions to the stiffness matrices and as such do not make the inversion more difficult.

The treatment of other terms could vary depending on tasks and numerical efficiency. Since we are interested in long integration periods, we treat all terms in the LHS of (15) and (16) implicitly, as it permits using large time steps. Implicitness implies that the systems of equations (15) and (16) are solved simultaneously for the vector $(\mathbf{u}_k, \zeta_k)$. We use the energy norm $\|(\mathbf{u}, \zeta)\| = \int \mathbf{u} \cdot \mathbf{u} \, \mathrm{d}\Omega + g \int \zeta^2 \, \mathrm{d}\Gamma_1$ obtained by adding (16) multiplied with the acceleration due to gravity g, to (15). This ensures that the potential energy due to the sea surface elevation would be properly accounted in the energy balance. To see that, take $\tilde{\mathbf{u}} = \mathbf{u}$ and $\tilde{\zeta} = \zeta$.

The pressure gradient term on the RHS of (15) is computed explicitly, because otherwise we have to solve the momentum, continuity and nonlinear tracer equations simultaneously, which is too costly. There are two options for computing the momentum advection term. It can be explicit or linearized (with only $\mathbf{u} \cdot \nabla + w \partial_z$ estimated at the preceding time step) and treated implicitly. The second option is safer and more accurate, but requires reassembling the stiffness matrix at every time step. We use the first option, as the momentum advection term is much smaller than ∇p which is considered explicitly. Although the RHS of (15) contains first-order derivatives, we have not noticed any related instability. To summarize, we integrate Eqs. (15) and (16) with the backward Euler scheme with explicit treatment of the momentum advection and hydrostatic pressure terms which are computed at the preceding time step.

The vector $(\mathbf{u}_k, \zeta_k)$ has dimension of $2N_{3\mathrm{D}} + N_{2\mathrm{D}}$, and inverting the stiffness matrix corresponding to the combined problem (15) and (16) creates the main numerical load. The stiffness matrix has strong antisymmetric part, so availability of efficient solvers could become a critical issue. Traditionally, FDMs split the problem into the barotropic and baroclinic parts, and solve separately for barotropic transports and baroclinic velocities. In that case the most difficult elliptic-type problem of computing the transports becomes 2D and could be solved easier. Given tetrahedral FEs, however, the vertically integrated horizontal velocity (transport) does not belong to the functional space of linear functions on surface triangles, as $\mathbf{u}$ does. This renders introducing transports not so straightforward as in the FDM. While this approach is in principle feasible with the FEM, its practical realization encounters problems, as explained in Appendix B.

The advection term is mainly balanced with the time derivative term in the tracer equations. So we treat it implicitly there to ensure stability in long runs, and integrate these equations in time with the backward Euler scheme. Although implicit advection requires reassembling the stiffness matrix at each time step, it does not create much computational burden because the time step of dynamical equations typically takes more CPU time (see the details of implementation in Section 5). The same stiffness matrix is used for time stepping temperature and salinity, or any other tracer included in the model. Thus increasing the number of tracers would reduce the relative cost of the assembly procedure.

The discretization of the primitive equations described above allows for integration of the model with reasonable values of the viscosity and time steps of up to few hours for the horizontal resolution of several tens km. However, due to accumulation of the small-scale numerical noise, the model trajectory degrades after a couple of years of integration (or the model should be made too dissipative from the very beginning).

The same behaviour of the SEOM is reported in Levin et al. (1997) unless a special filtering procedure was applied. The problem of damping the numerical noise and still having a low viscosity to simulate turbulent ocean flows is a crucial issue for OGCMs. In addition to using improved advection schemes, the vast majority of the OGCMs employs the biharmonic horizontal friction operator instead of the traditional Laplacian friction because of scale-selective properties of the former. However, implementation of the hyperviscosity in the FEM is problematic since it requires using basis functions which would be not only continuous across the element borders but also continuously differentiable. For a tetrahedral mesh, the minimal set of such basis functions are polynomials of the fifth order which are far too expensive to be used for meshes having $O(10^6)$ elements. We utilize here another approach described in Section 4.

4. Stabilization

The FEM using linear basis functions due to its central difference property is well suited only for solving elliptic problems (dominated by the diffusion). In the ocean, the evolution of the temperature and salinity is mainly governed by the advection that is dominating over the diffusion. This causes numerical problems.

Let us consider for simplicity a stationary advection–diffusion equation

$$\mathbf{u}\cdot\nabla T - k\Delta T = F, \quad (x,y)\in\Omega, \tag{23}$$

$$k\frac{\partial T}{\partial n} = q, \quad (x,y)\in\partial\Omega, \tag{24}$$

in a 2D domain Ω with the boundary $\partial\Omega$. Here F is a source term and k is a diffusion coefficient, q is the temperature flux taken with opposite sign, and the derivative in (24) is taken in the direction of the outer normal. For a given velocity field $\mathbf{u}$ such that $\nabla\cdot\mathbf{u}=0$ and $\mathbf{u}\cdot\mathbf{n}=0$ at $\partial\Omega$,

$$\int_\Omega T(\mathbf{u}\cdot\nabla T)\,\mathrm{d}\Omega = 0, \tag{25}$$

and thus the stability of the Galerkin method applied to solving (23) relies entirely on $k\|(\nabla T)\|^2$ that can be small for very small k. The stiffness matrix that corresponds to the problem (23) and (24) is essentially non-symmetric and difficult to invert, while the solution to the problem could exhibit spurious oscillations.

Problems of the same origin arising in modelling advection-dominated flows, i.e. when the mesh-Peclet number $Pe = |\mathbf{u}|h/k$, where h is the grid step, is large, are well known in the FD literature. Pacanowski and Griffies (2000) mentioned that if $Pe > 2$, MOM will not necessarily blow-up but the solution will slowly degrade with time stepping. A way around this problem is to add some artificial diffusivity to ensure $Pe < 2$ (Bryan et al., 1975) that makes the solution too dissipative. Otherwise, it will exhibit spurious oscillations of the wavelength proportional to the grid size (as in standard central differences). The other (already mentioned) way to tackle this problem is using more sophisticated advection schemes (Webb et al., 1998; Hecht et al., 2000) that exploit higher-order spatial approximations.

The problem attracted much attention over the last two decades in the FE literature and several recipes how to make the problem better posed and avoid adding much diffusivity were put for-

ward. A substantial progress in this direction was achieved after recognition that the original problem may be transformed to a new one with much better properties in such a way that the solution to the former will also be the solution to the latter. Seemingly, the most general among these so-called residual free methods is the GLS (Hughes et al., 1989) utilized in the model described here.

4.1. Stabilization for the thermodynamical part

The idea behind the GLS stabilization is simple: one modifies the original differential equations in such a way that the solution would satisfy both the original and the modified equations while the discretization of the latter would produce a matrix whose inversion would require less iterations of an iterative solver. If we consider (23), the diffusion term for small k is important only in the narrow boundary layer of the width of $O(k/|\mathbf{u}|)$ and is effectively dropped in the discretized equations when $h \gg k/|\mathbf{u}|$. Eq. (23) almost corresponds to the first-order differential advection operator that does not need boundary conditions along the whole boundary $\partial\Omega$. Hence, the problem becomes nearly overdetermined. What is needed to restore the well-posedness of the problem is to increase the order of the dominant differential operator.

For any sufficiently smooth $\widetilde{T}$, the solution T to the problem (23) and (24) satisfies the following integral equality

$$\int_\Omega [\widetilde{T}(\mathbf{u}\cdot\nabla T) + k\nabla\widetilde{T}\cdot\nabla T]\,\mathrm{d}\Omega = \int_\Omega \widetilde{T}F\,\mathrm{d}\Omega + \int_{\partial\Omega} q\widetilde{T}\,\mathrm{d}|\partial\Omega|, \tag{26}$$

that is a starting point in deriving Galerkin equations. We may modify (26) and write down an equivalent equality

$$\int_\Omega [\widetilde{T}(\mathbf{u}\cdot\nabla)T + k\nabla\widetilde{T}\cdot\nabla T]\,\mathrm{d}\Omega + \int_{\Omega_1} \varepsilon_t(\mathbf{u}\cdot\nabla - k\Delta)\widetilde{T}(\mathbf{u}\cdot\nabla T - k\Delta T - F)\,\mathrm{d}\Omega$$
$$= \int_\Omega \widetilde{T}F\,\mathrm{d}\Omega + \int_{\partial\Omega} q\widetilde{T}\,\mathrm{d}|\partial\Omega|. \tag{27}$$

Here $\Omega_1 \subset \Omega$ is an arbitrary subdomain where T and $\widetilde{T}$ are twice differentiable, and ε_t is an arbitrary integrable function. The second integrand in the LHS of (27) is referred to as the stabilization term. The variational principles are completely equivalent. Therefore, instead of using (26) for deriving the set of discrete Galerkin equations, we can employ (27) that leads to the GLS stabilization.

If we consider the space of piecewise linear functions X_k for T and $\widetilde{T}$, then Ω_1 cannot be extended to the whole domain Ω but only to the sum of elements interiors $\cup E_1$. Within element interiors, functions T and $\widetilde{T}$ are analytical functions and $\Delta T = \Delta\widetilde{T} = 0$. Then, the stabilized weak formulation of the problem (23) and (24) can be written as

$$\int_\Omega [\widetilde{T}(\mathbf{u}\cdot\nabla T) + k\nabla\widetilde{T}\cdot\nabla T]\,\mathrm{d}\Omega + \int_{\cup E_1} \varepsilon_t(\mathbf{u}\cdot\nabla\widetilde{T})(\mathbf{u}\cdot\nabla T - F)\,\mathrm{d}\Omega$$
$$= \int_\Omega \widetilde{T}F\,\mathrm{d}\Omega + \int_{\partial\Omega} q\widetilde{T}\,\mathrm{d}|\partial\Omega|. \tag{28}$$

The proper choice of the stabilization parameter ε_t in the stationary case has been thoroughly discussed in the FE literature. The general recipe is to take $\varepsilon_t = O(h/|\mathbf{u}|)$ for $Pe \gg 1$ and $\varepsilon_t = O(h^2/k)$ for small Peclet numbers (Hughes et al., 1989).

Extension of the GLS to the original problem of non-stationary tracer evolution is straightforward:

$$\int_\Omega [\widetilde{T}(\partial_t + \mathbf{u}\cdot\nabla + w\partial_z)T + A_l\nabla\widetilde{T}\cdot\nabla T + A_v\partial_z\widetilde{T}\,\partial_z T]\,d\Omega + \int_{\cup E_l} \varepsilon_t(\mathbf{u}\cdot\nabla + w\partial_z)\widetilde{T}(\partial_t T + \mathbf{u}\cdot\nabla T + w\partial_z T - F)\,d\Omega = \int_\Omega \widetilde{T}F\,d\Omega + \int_{\partial\Omega} q\widetilde{T}\,d|\partial\Omega|, \tag{29}$$

that should be satisfied for any piecewise linear function $\widetilde{T}$. Here q stands for surface and open boundary diffusive fluxes of T. The tracer stabilization parameter ε_t is computed for each element with horizontal and vertical dimensions h and Δz respectively, from

$$\varepsilon_t = [1/\Delta t + 4A_l/h^2 + 2A_v/\Delta z^2 + |\mathbf{u}|/h + |w|/\Delta z]^{-1}. \tag{30}$$

Here Δt is the time step for the tracer problem. The expression (30) is interpolation between limits of large and small Peclet numbers. The contribution from Δt in non-stationary case follows from an approach to stabilized equations proposed in Ilinka et al. (2000) (see also Appendix A for further discussion).

Several comments could be made with respect to the stabilization algorithm of the advection–diffusion problem. First, there is similarity with upwind scheme, yet it is superficial. The stabilization does not introduce the upwind diffusion, as the upwind term is approximately balanced with other terms almost everywhere excluding regions of very high temperature gradient. We analyze the dispersion properties of the stabilized advection–diffusion equation in Appendix A and show that the stabilization introduces negligible dissipation at large scales and strongly damps the smallest resolved scales, as expected. It also reduces dispersion if the stabilization parameter is appropriately chosen. Second, the same stabilization could be derived using bubble functions and minimizing the residual on elements (residual-free bubbles method, see Brezzi et al., 1996). This approach was used in Nechaev et al. (2003). Third, to some extent, it can be viewed as parameterization of unresolved (by basis functions) subgrid scales (for detail, see Hughes, 1995).

4.2. Stabilization for the dynamical part

Large-scale ocean dynamics is nearly in geostrophic balance. Consequently, one encounters the same numerical problem as that described above for the advection–diffusion equation if the horizontal resolution is too coarse to resolve the viscous boundary layer, i.e. if the local Ekman number $Ek = (2A_l/f)^{1/2}/h$ is small. Indeed, if we multiply the steady-state version of (1) by $\mathbf{u}$, take into account (2) and boundary conditions and consider a flat bottom case with $\tau = 0$ and $C_g = 0$ for simplicity, then we arrive at

$$A_v\|\partial_z\mathbf{u}\|^2 + A_l\|\nabla\mathbf{u}\|^2 = -\rho_0^{-1}\int_\Omega \nabla p\cdot\mathbf{u}\,d\Omega, \tag{31}$$

and again notice that the stability of the problem completely relies on the small values of viscosity coefficients A_l, A_v, as the RHS of (31) is not sign definite.

In addition, there is one more difficulty that is specific to the FE discretization of the Navier–Stokes and primitive equations. It is well known that FE spaces $\mathbf{V}_h$ and Q_h for the velocity and the pressure, respectively, cannot be chosen arbitrary if the standard Galerkin method is applied to modelling incompressible flows. They have to meet the so-called Babuška–Brezzi–Ladyzhenskaya condition (BBL) (Babuška, 1973; Brezzi, 1974; Ladyzhenskaya and Solonnikov, 1976). Piecewise linear basis functions for the velocity and pressure do not meet this requirement. Violating the BBL condition results in spurious null-space surface-elevation solutions.

Both numerical problems can be resolved with the GLS (Codina and Soto, 1997). Introducing $\mathbf{L} = \partial_t \mathbf{u} + f\mathbf{k}\times\mathbf{u} + g\nabla\zeta$, $\mathbf{L}_1 = \nabla A_1 \nabla \mathbf{u} + \partial_z A_v \partial_z \mathbf{u}$ and denoting by $\mathbf{R}$ the terms on the RHS of (1) we write the stabilized equations as

$$\int_\Omega (\mathbf{L}\cdot\tilde{\mathbf{u}} + A_1\nabla\mathbf{u}\cdot\nabla\tilde{\mathbf{u}} + A_v\partial_z\mathbf{u}\cdot\partial_z\tilde{\mathbf{u}})\,d\Omega + \int_{\Omega_1}\varepsilon_d f(\mathbf{L}+\mathbf{L}_1)\cdot(\mathbf{k}\times\tilde{\mathbf{u}})\,d\Omega_1$$
$$= \int_\Omega \mathbf{R}\cdot\tilde{\mathbf{u}}\,d\Omega + \int_{\Omega_1}\varepsilon_d f\mathbf{R}\cdot(\mathbf{k}\times\tilde{\mathbf{u}})\,d\Omega + \int_{\Gamma_1}\boldsymbol{\tau}\cdot\tilde{\mathbf{u}}\,d\Gamma_1 - \int_{\Gamma_2} C_g|\mathbf{u}|\mathbf{u}\cdot\tilde{\mathbf{u}}\,d\Gamma_2,$$
$$\int_{\Gamma_1}\partial_t\zeta\tilde{\zeta}\,d\Gamma_1 - \int_\Omega \nabla\tilde{\zeta}\cdot\mathbf{u}\,d\Omega + \int_{\Omega_1}\varepsilon_d\nabla\tilde{\zeta}\cdot(\mathbf{L}+\mathbf{L}_1-\mathbf{R})\,d\Omega_1 + \int_{\Gamma_4}\tilde{\zeta}\mathbf{v}_{OB}\cdot\mathbf{n}\,d\Gamma_4 = 0.$$

Here ε_d is the stabilization parameter. The stabilization terms in both equations contain contributions from viscous terms $\mathbf{L}_1$ which are zeros on linear functions inside the elements. In the standard approach (applied when the problem is posed with the Dirichlet boundary conditions), one extends integration only to the element interiors thus omitting $\mathbf{L}_1$ in the stabilization. In our case the problem is set with the two Neumann boundary conditions at Γ_1 and Γ_2 that correspond to essential forcing and (less essential) dissipation shaping the entire flow. To properly take them into account we should make one step back and consider the two equations above as formulation of a weak problem with yet unspecified (but sufficiently smooth) fields, test functions and ε_d. We then integrate by part contributions from dissipative terms in stabilization and return to linear functions, extending Ω_1 to the sum of element interiors and considering ε_d to be elementwise constant. (Note that the Neumann boundary conditions in tracer equations do not require special attention in the rigid lid case because boundaries are impermeable.)

The stabilized equations expressing the momentum and mass conservation take the form

$$\int_\Omega (\partial_t\mathbf{u} + f\mathbf{k}\times\mathbf{u} + g\nabla\zeta)\cdot(\tilde{\mathbf{u}} + \varepsilon_d f\mathbf{k}\times\tilde{\mathbf{u}})\,d\Omega + \int_\Omega (A_v\partial_z\mathbf{u}\cdot\partial_z + A_1\nabla\mathbf{u}\cdot\nabla)(\tilde{\mathbf{u}} + \varepsilon_d f\mathbf{k}\times\tilde{\mathbf{u}})\,d\Omega$$
$$= -\rho_0^{-1}\int_\Omega \nabla p\cdot(1+\varepsilon_d f\mathbf{k}\times)\tilde{\mathbf{u}}\,d\Omega + \int_{\Gamma_1}\boldsymbol{\tau}\cdot(1+\varepsilon_d f\mathbf{k}\times)\tilde{\mathbf{u}}\,d\Gamma_1 - \int_{\Gamma_2} C_g|\mathbf{u}|\mathbf{u}\cdot(1+\varepsilon_d f\mathbf{k}\times)$$
$$\times\tilde{\mathbf{u}}\,d\Gamma_2 - \int_\Omega (1+\varepsilon_d f\mathbf{k}\times)\tilde{\mathbf{u}}\cdot(\mathbf{u}\cdot\nabla + w\partial_z)\mathbf{u}\,d\Omega, \tag{32}$$

$$\int_{\Gamma_1}\partial_t\zeta\tilde{\zeta}\,d\Gamma_1 - \int_\Omega \mathbf{u}\cdot\nabla\tilde{\zeta}\,d\Omega + \int_\Omega \varepsilon_d\nabla\tilde{\zeta}\cdot(\partial_t\mathbf{u} + f[\mathbf{k}\times\mathbf{u}] + g\nabla\zeta + \rho_0^{-1}\nabla p + (\mathbf{u}\cdot\nabla + w\partial_z)\mathbf{u})\,d\Omega$$
$$-\int_{\Gamma_1}\varepsilon_d\boldsymbol{\tau}\cdot\nabla\tilde{\zeta}\,d\Gamma_1 + \int_{\Gamma_2}\varepsilon_d C_g|\mathbf{u}|\nabla\tilde{\zeta}\cdot\mathbf{u}\,d\Gamma_2 + \int_{\Gamma_4}\mathbf{v}_{OB}\cdot\mathbf{n}\,d\Gamma_4 = 0. \tag{33}$$

The stabilization parameter for the dynamical problem ε_d is computed from

$$\varepsilon_d = [|f| + (\Delta t)^{-1} + 10A_1/h^2]^{-1}, \tag{34}$$

where Δt is the time step of the dynamical problem. Expression (34) is interpolation between two limiting cases of small and large Ekman numbers. In the first case, for the steady-state problem Codina and Soto (1997) recommend $\varepsilon_d = |f|^{-1}$. Accounting for non-stationarity can be done following the approach of Ilinka et al. (2000). The third term in (34) corresponds to the asymptotics of ε_d in the diffusive limit ($Ek \gg 1$) derived in Nechaev et al. (2003). Codina and Soto (1997) recommend the factor of 12 (instead of 10) in this term based on their numerical experiments.

For Δt and h used in the model and for typical values of horizontal diffusivity $\varepsilon_d \approx |f|^{-1}$. Thus, the difference between the original (15) and stabilized (32) momentum equations is that the latter is a linear combination of the former and its rotation and the stabilization of the momentum equations is an algebraic operation on the original Galerkin equations. If we consider a block of the stiffness matrix corresponding to the velocity–velocity part of the momentum equations, the stabilization can be illustrated schematically as that instead of inverting the matrix

$$\begin{pmatrix} D+T & -f \\ f & D+T \end{pmatrix},$$

where D, T and f denote blocks that correspond to discretization of the viscosity, time derivative and Coriolis parts respectively, we provide the solver with the matrix

$$\begin{pmatrix} D+T+f & D+T-f \\ f-D-T & D+T+f \end{pmatrix}$$

that is much better from the computational point of view when dissipation is small and the time step is large. Indeed, its symmetric and antisymmetric parts are of comparable magnitude, which provides faster convergence of iterative solvers.

This is in contrast with the stabilized continuity equation (33) that contains an additional term. This term would coincide with the divergence of the z-integral of the residual in the momentum equation if the viscous terms were included into stabilization in (33). Then it would be equal to zero. However, working in the space of piecewise linear basis functions we are unable to compute them and consequently have to admit an error of the order $O(Ek)$ in the continuity equation. Hence, the flow field resulting from solving (32) and (33) possesses a non-trivial 2D divergence and thus is not volume conserving. This issue is addressed below. Noteworthy, the same stabilization of the continuity equation without introducing the stabilization term in the momentum equation is considered in Hanert et al. (2003).

4.3. Velocity correction for recovering the volume conservation

A common viewpoint (see, for example, Ilinka et al., 2000) on the problem of breaking the volume conservation by stabilization of the dynamical equations in the FEM is as the following. Expressing the unknown model variables as a linear combination of a finite set of basis functions one is able to compute only a part of the total fields. Stabilization parameterizes the contribution from the unresolved (by the basis functions) part. It is the total field that must satisfy the

governing equations while the solution obtained by solving the stabilized equations represents only a part of the total field and does not have to fit the continuity equation exactly.

In ocean circulation modelling, we are interested not only (and primarily not) in the velocity field but in the transport of ocean tracers that cannot be computed from the 3D velocities obtained from (32) and (33). Indeed, if we tried to compute w from (7), it would be impossible to meet both boundary conditions at the bottom and at the surface. In other words, the RHS of (7) would not meet the solvability condition. Hence, advecting the tracers we would produce uncontrolled surface and/or bottom fluxes which could degrade the solution in a long term run. Thus, we need to trim the horizontal velocity field so that it would satisfy the continuity constraint (would have zero 2D divergence).

However, (33) does not suggest introducing a 3D field of correcting horizontal velocity, as it operates with vertically integrated quantities. In fact, an attempt to compute it would lead to extremely noisy field that cannot be used.

A scheme similar to that proposed by Deleersnijder (2001) was adopted. After solving the stabilized equations, the 2D potential ϕ is computed by solving

$$\Delta\phi = \nabla \cdot \int \mathbf{u}\,\mathrm{d}z, \quad \partial_n\phi = 0. \tag{35}$$

This equation is treated in the weak sense in the space of piecewise linear basis functions $\phi = \sum \pi_k S_k$ Once ϕ has been computed, the bias $\nabla\phi$ is extracted from the horizontal velocity field

$$\mathbf{u} \to \mathbf{u} - H^{-1}\nabla\phi. \tag{36}$$

Here H is the local depth.

As we have already mentioned the local residual in the original continuity equation (2) is of the order $\mathrm{O}(Ek)$ and thus this potential part of the flow should be small for the oceanic currents. Indeed, as computations revealed, the correction $H^{-1}\nabla\phi$ is a tiny fraction of the total velocities $\mathbf{u}$ and introduces a very small imbalance in the momentum conservation while allowing the mass conservation to be recovered. The correction is especially small in the exterior of boundary tetrahedra and typically is of the order 10^{-6} m/s. The corrected velocity field is further used for computing w and advecting the tracer fields and momentum.

4.4. Tracer conservation properties of the model

The way in which the 3D continuity equation (20) is solved for the vertical velocity w ensures, as we have already mentioned, that volume is conserved locally when summed over the cluster of tetrahedra spanned by a test function, and globally. It also plays the crucial role in providing the conservation properties of the tracer equations. Indeed, the total tracer contained in the volume should be conserved provided total flux of the tracer through the boundaries is zero and sources are absent. The stabilized FEM tracer equation (29) satisfies this constraint. Indeed, if we take $\widetilde{T} = \text{const}$ in (29), which is equivalent to the volume integration, the advection terms of the tracer equation reduce to

$$\int_\Omega (\mathbf{u}\cdot\nabla + w\partial_z)T\,\mathrm{d}\Omega = 0.$$

The latter is ensured by (20) for any elementwise linear field T (the surface integral in (20) gives zero total transport because of volume conservation). Then it follows from (22) that

$$\partial_t \int_\Omega T \, d\Omega = 0.$$

We would like to emphasize that stabilization does not affect the global tracer conservation property, as the stabilization terms in (29) contain only derivatives of $\widetilde{T}$ and vanish for $\widetilde{T} =$ constant.

In FD modelling the advection equation is usually written in the flux form to ensure the global tracer conservation. With the FEM, the global conservation is the consequence of the weak (Galerkin) formulation and the scheme of computing the vertical velocity.

For the same reason as the tracer advection term, the momentum advection term in the momentum equation goes to zero after having being integrated over the volume. This is once again a desirable property, as this term should only redistribute the momentum and cannot create or destroy it.

5. Finite-element model of North Atlantic (FENA)

The model performance was tested using the North Atlantic setup. The computational mesh covers the region from 7° to 80° N. It is based on a surface triangular mesh consisting of 6480 surface nodes, and a combination of z and σ-levels in the vertical direction. Each surface triangle defines a vertical prism which is subdivided by level surfaces into elementary prisms. The latter are split into tetrahedra. The surface mesh defines horizontal resolution, which varies from 0.3° to 1.5°, with mean of approximately 0.8°. Using the combination of z and σ levels (with total of 16 levels) allows us to get rid of vertical walls in the volume of water and simultaneously reduce the total number of 3D nodes compared to purely σ-level setup. The total number of 3D nodes is 86 701, and they form 449 674 tetrahedra. Figs. 1 and 2 present views of 2D and 3D discretizations

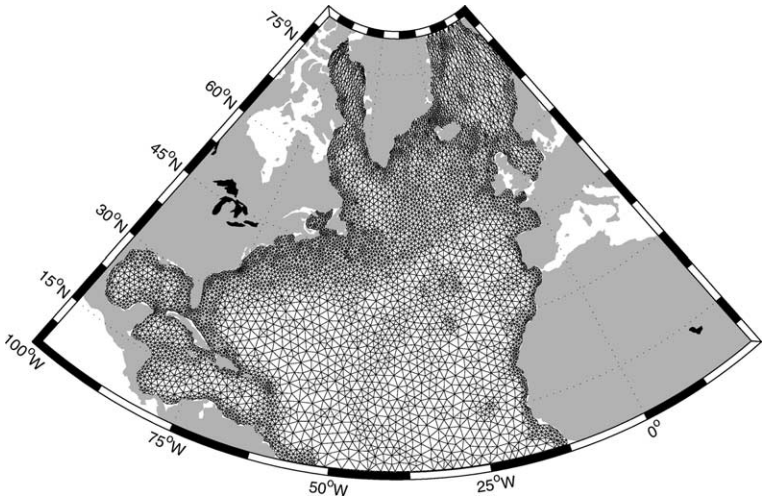

Fig. 1. 2D mesh of FENA model.

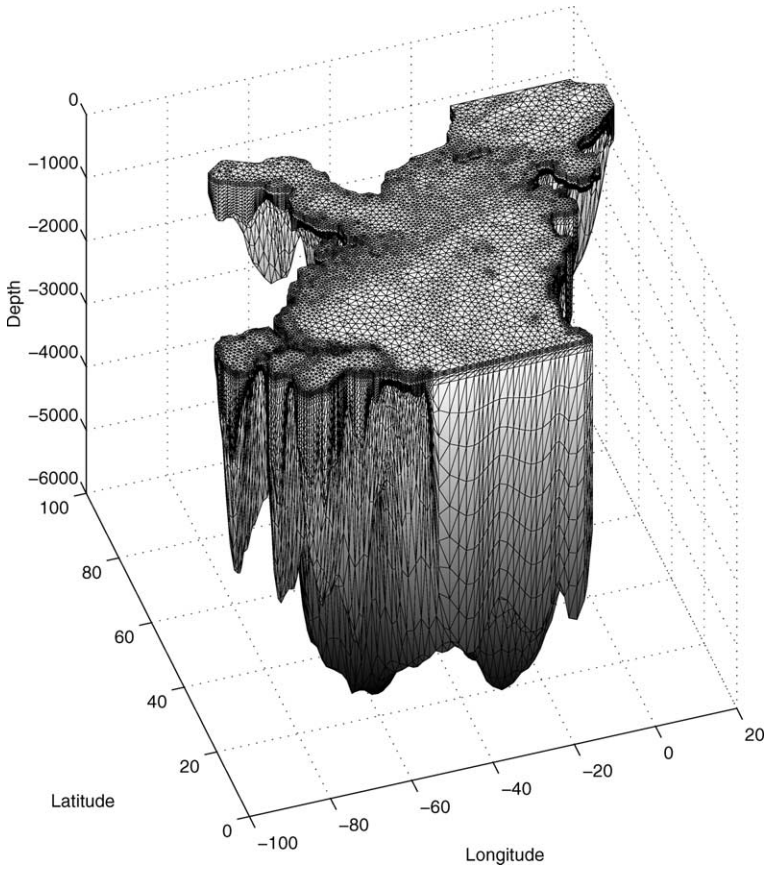

Fig. 2. View on 3D FE mesh of FENA model.

used in the model. They clearly demonstrate the main advantage of FE—their ability to provide local mesh refinement only in the locations where it is indeed necessary.

The model was forced at the surface by the monthly mean climatological wind stress (Trenberth et al., 1989). The surface temperature and salinity were restored to the Levitus monthly data with the relaxation time of 15 days. The model was run for 16 years with time step of $\Delta t = 12$ h for the dynamical part and a reduced time step $\Delta t/n$ for the tracer part. Here n is the number of steps for tracers within one time step of dynamical part. The tracer stiffness matrix is reassembled each time after the dynamical part is stepped forward, and kept constant during n tracer steps. Typically $n = 4$, but increasing it would not affect the CPU time significantly (see below).

Numerical implementation of solver uses parallel threshold-based ILU factorization (Karypis and Kumar, 1997) and GMRES or BICGSTAB algorithms. The memory required by the solver and pre-conditioner and the efficiency of the solver depend on how many fill-in elements are allowed for the factorization. Increasing the number of fill-in elements reduces the number of iterations needed to provide the convergence of the solver, but requires additional storage and increases the number of numerical operations during an iteration. The "optimal" fill-in number is mainly sensitive to the band width of the sparse matrix to be inverted. With increasing the band

width it also increases if the acceptable number of iterations is bounded. A helpful approach is renumbering the nodes to reduce the bandwidth of the stiffness matrix, so that the ILU-factorization would need less fill-in elements and/or require less iterations to converge (Dobrindt and Frickenhaus, 2000). As we saw, too large difference between numbers of neighbouring nodes could locally degrade or even totally destroy the solution with time stepping. The reordering can be made with the Metis package (Karypis and Kumar, 1998) which also provides a tool for partitioning the mesh needed for implementation of parallel solvers. For the current version of the model the fill-in numbers from 100 to 200 provide convergence of the dynamical part typically within 10 iterations. Tracer advection–diffusion problem converges within 3–4 iterations with fill-in between 35 and 50.

Within a time step Δt, the solution of dynamic problem takes about 25%, and another 25% are required to assemble and factorize the stiffness matrix for the tracer problems. It is worth to notice that assembling the stiffness matrix and the RHSs is a highly parallelizable procedure. Given partitioning of the mesh, each processor deals with its own part of the matrix and the RHS and they communicate only at the factorization/solution step. Since the assembly of the stiffness matrix and its factorization are costly tasks, they are performed for the stiffness matrix of the tracer part once per the time step of the dynamical part. Assembling RHSs of the tracer (temperature and salinity) equations and solving them $n = 4$ times requires less time than the assembly and factorization of the stiffness matrix, so the parameter n is not highly critical.

The stiffness matrix of the dynamical problem is not varying with time if viscosity is kept fixed. In such a case it is assembled and factorized only once. The stiffness matrices for the vertical velocity and correcting potential are also assembled and factorized only once.

The current version of FENA is supplied with a Smagorinsky-type viscosity in the momentum equation. The horizontal viscosity is prescribed the Smagorinsky-type value at those elements where the latter is in excess of $A_l = 200$ m^2/s. The vertical viscosity is fixed at $A_v = 0.002$ m^2/s, while diffusivities in tracer equations take values of $K_l = 200$ m^2/s and $K_v = 0.0002$ m^2/s. Numerical implementation of time-varying horizontal viscosity requires updating the stiffness matrix at each time step. To spare time, we skip the refactorization step, as the main part of the stiffness matrix (responsible for the geostrophic balance) remains intact. Although updating the stiffness matrix requires considerable time within a time step, it allows simulations with the horizontal viscosity coefficient as low as $A_l = 200$ m^2/s almost everywhere except for close proximity of coastal zones and strong currents. It should be recalled that the stabilization of momentum equation cannot regularize the velocity field in the regions where the spatial resolution is not sufficient, as it is largely an algebraic operation (see Section 4). Thus augmented (Smagorinsky) explicit viscosity is needed there. The stabilization of tracer equations solves problems of that kind, and does not require increased diffusivity in such regions.

In a current implementation, a model year requires 8 h of CPU time on four processors of SGI ORIGIN-2000.

Fig. 3 shows a snapshot of temperature and velocity field in the region of the Gulf Stream at the end of the integration time. Noteworthy is the wavy structure of the current and its separation off the coast at approximately 40° N. Although there is a tendency to eddying in the velocity field, it is only marginally present, as the spatial resolution is still insufficient on the offshore side of the Gulf Stream. The same type of behaviour could be seen in the snapshot of the sea surface height presented in Fig. 4. Given mean spatial resolution of 0.8° this behaviour is indeed encouraging.

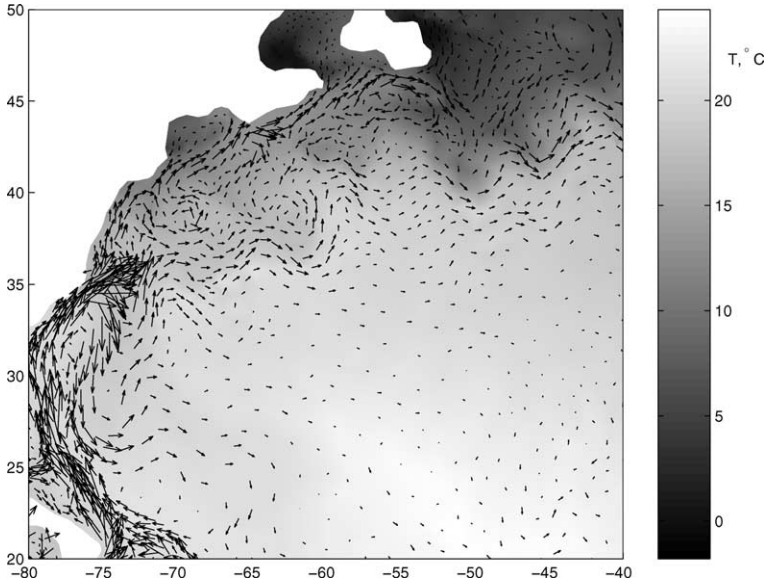

Fig. 3. Velocity and temperature (gray scale color) fields after 16 years of integration of FENA model at the location of Gulf Stream (at the depth of 100 m). The maximum velocity amplitude is 0.7 m/s.

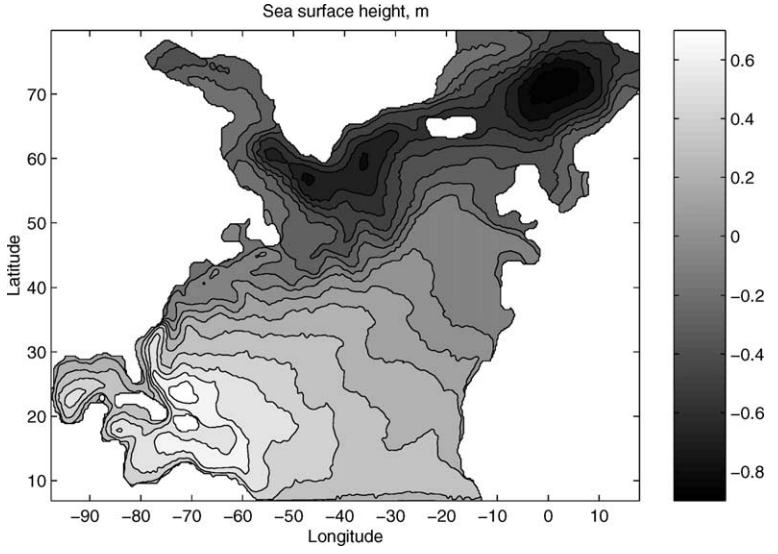

Fig. 4. The sea surface height at the end of the run (drawn via interpolation to a regular grid).

No relevant treatment was given to the open boundaries in the current version of the model, as only its performance was tested. The open boundaries were treated as closed. This entails unrealistic details in the circulation in regions neighboring the open boundaries. However, as we have already mentioned, there is no mathematically consistent way to treat them, and perhaps the best

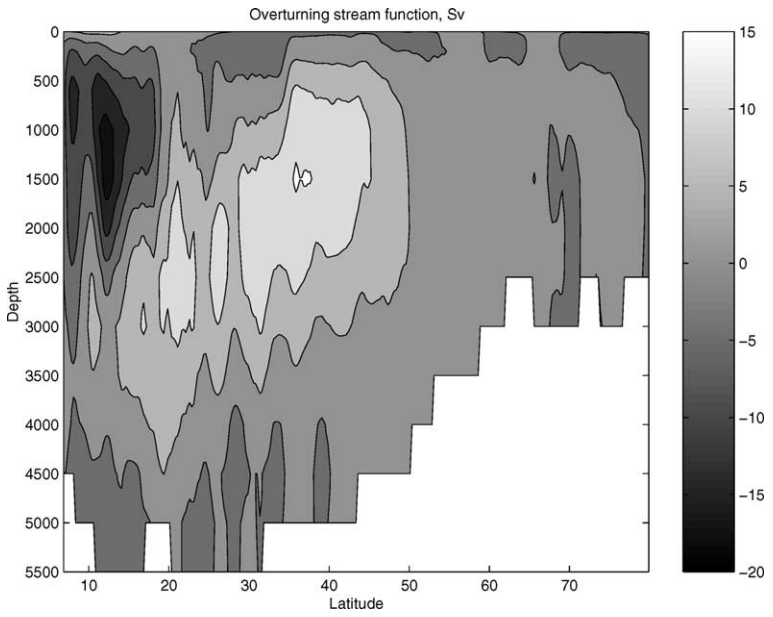

Fig. 5. The meridional overturning stream function produced by FENA model (obtained by interpolating the velocity on a regular grid, computing velocity curl and solving the Poisson equation for the overturning stream function).

recipe is to have them as far as possible from the region of interest. No special care was given to reproducing particular details of bottom topography, which is responsible for some errors in the circulation in the Caribbean basin. Despite all that, such global characteristics of the model as its overturning stream function (Fig. 5) and meridional heat transport (Fig. 6) compare well with the other estimates obtained with models of comparable resolution (see Chassignet et al., 2000; Haidvogel et al., 2000). The maximum of the overturning stream function is about 20 Sv, and typical amplitudes of the meridional heat flux are of the order of 0.8 PW.

6. Conclusions

The FE model intended for simulating OGC is described. The model is further development of the diagnostic FE model by Nechaev et al. (2003), and differs from it in several important aspects such as time-stepping, GLS stabilization, divergence correction, time-dependent (Smagorinsky-type) viscosity, and others. The model performance is stable and the model skill was tested in the 16-year run in the North Atlantic setup. The suite of tests of model performance and accuracy in elementary setups (such as, for example, the Munk problem, the elementary overflow problem in the DOME experiment geometry) will be presented in a separate paper.

Using FE with 3D tetrahedral partitioning and linear functions for the sea surface height and horizontal velocity suggests a different (compared to FD) way of thinking of OCM, and the standard recipe such as splitting the velocity field into barotropic and baroclinic parts, could not be used directly, because the fields of velocity and vertically integrated velocity (transport) belong

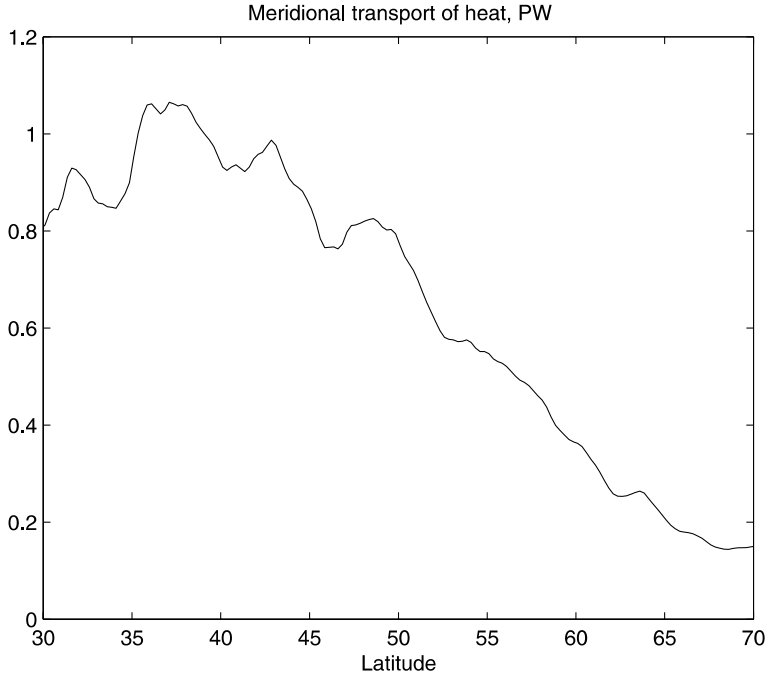

Fig. 6. Meridional heat transport corresponding to the overturning circulation in the previous figure. Computed via interpolation of velocity and temperature on the regular grid.

to different spaces (of linear and cubic functions respectively). One can still solve the vertically integrated equations for transports and the sea surface height ζ, and use this information as described in Appendix B. While formally attractive, splitting is difficult to implement, as it requires explicit correction of dissipation terms in equations for vertically integrated fields, which turns to be too noisy for unstructured meshes. Further work in this direction is needed.

There are other directions for future work as well, and the most promising one is adaptation of the model to the global ocean with refinement of the grid in regions of interest. Augmenting the model with a set of tracer equations could be of interest for applications in biology. Their integration would be efficient as it would use the stiffness matrix already assembled and factorized to integrate the equations for temperature and salinity.

Acknowledgements

The FE model presented here is a development of the "Inverse Modeling Group" of the Department "Climate Systems" at Alfred Wegener Institute in Bremerhaven, Germany. At different stages several people contributed to programming the code: Dmitri Nechaev, Uwe Dobrindt, Sven Harig and the authors. Support of Stephan Frickenhaus in parallelization of the code and efficient implementation of solvers for large linear systems was extremely valuable. We are also grateful to Alexandre Kurapov (Oregon State University) for providing us with a mesh generation code.

Appendix A. Dispersion properties of the stabilized advection–diffusion equation

It is instructive to analyze the dispersion relations of stabilized FE advection–diffusion equation and compare it with other schemes of FD origin. As is common with such type of analyses, we consider the 1D advection–diffusion equation with a constant advecting velocity u. In the FE setup, we first write it in a weak formulation

$$\int (\partial_t T\widetilde{T} + u\,\partial_x T\widetilde{T} + K\,\partial_x T\,\partial_x \widetilde{T} + \varepsilon_t u\,\partial_t T\,\partial_x \widetilde{T} + \varepsilon_t u^2\,\partial_x T\,\partial_x \widetilde{T})\,\mathrm{d}x = 0,$$

assuming that ε_t is constant, and choose T and $\widetilde{T}$ belonging to the space of linear (on elements) functions. Given a uniform 1D grid with element size $h = 1$ the FE discretized equation reduces to the following equation on nodal values of the tracer field T:

$$\partial_t(T_{n-1} + 4T_n + T_{n+1})/6 + \varepsilon_t u\,\partial_t(T_{n-1} - T_{n+1})/2 + u(T_{n+1} - T_{n-1})/2 + (K + \varepsilon_t u^2)(2T_n - T_{n+1} - T_{n-1}) = 0.$$

Seeking the solutions to this equation in the form of waves $\mathrm{e}^{-\mathrm{i}\omega t + \mathrm{i}kx}$ we obtain the dispersion relation

$$\omega h/u = \frac{6\sin kh}{4 + 2\cos kh - 6\mathrm{i}\bar{\varepsilon}_t \sin kh} - 6\mathrm{i}(\bar{\varepsilon}_t + Pe^{-1})\frac{2 - 2\cos kh}{4 + 2\cos kh - 6\mathrm{i}\bar{\varepsilon}_t \sin kh},$$

where $\bar{\varepsilon}_t = \varepsilon_t u/h$ is non-dimensional stabilization coefficient, and $Pe = uh/K$ is the element Peclet number.

The dispersion relation is compared to the dispersion relations of central differences and the QUICK schemes (see Webb et al., 1998) in Fig. 7. The labeled curves in Fig. 7 refer to the fol-

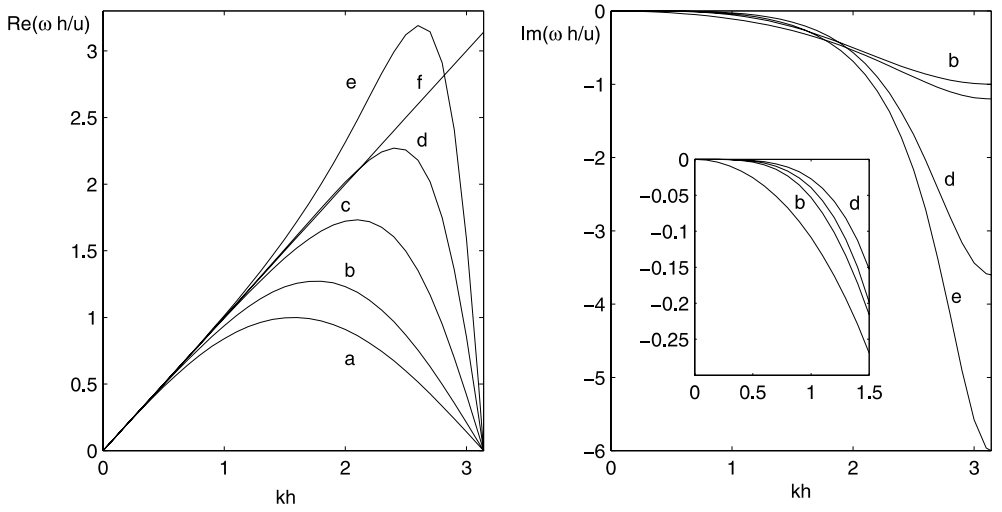

Fig. 7. Dispersion curves for several advection schemes: (a) central differences, (b) QUICK, (c) FE without stabilization, (d, e) FE with $\bar{\varepsilon}_t = 0.3$ and 0.5; $Pe^{-1} = 0$ in (a)–(e). The straight line (f) in the left panel corresponds to the exact dispersion relation $\omega = uk$. The thin curve in the right panel presents dissipation for the FE case with $Pe = 10$ and no stabilization. The inset zooms into the region of small decrements.

lowing cases: central differences (a), QUICK (b), FE without stabilization (c), FE with $\bar{\varepsilon}_t = 0.3$ (d) and 0.5 (e); Pe^{-1} is set to 0. The straight line (f) corresponds to the exact dispersion relation $\omega = uk$. Unlabelled (thin) curve in the right panel of Fig. 7 presents dissipation for the FE case without stabilization, with $Pe = 10$. The inset in the right panel visualizes the region of small decrements.

Even in the absence of stabilization, the FE advection scheme (c) exhibits notably less dispersion than central differences (a) and QUICK (b). Adding "optimal" stabilization (d) further improves the behaviour of $Re(\omega)$. Increasing the stabilization parameter to 0.5 (e) still results in a scheme with good dispersive properties. Further increase is not recommended as it reduces the interval of wave numbers where real part of ω is close to uk.

The right panel shows imaginary part of frequency. Cases (d) and (e) have smaller dissipation than QUICK at $kh < \pi/2$, however they dissipate small scales ($kh > 2\pi/3$) more efficiently. Although standard diffusion with $Pe = 10$ (the thin line in the right panel) introduces stronger dissipation at large scales than the stabilization in cases (d) and (e), achieving the dissipation comparable with that of (d) and (e) at small scales would require Pe of several units and make scales around $kh = \pi/2$ too dissipative. On the other hand, if the stabilization and physical diffusion are both included, and the Peclet number is sufficiently high, the physical diffusion would only be seen at large scales, while small scales would mainly feel the numerical dissipation.

To conclude the analysis we note that the difference between the stabilization considered and the upwind stabilization is in the imaginary term in the denominator of the equation for ω. At small kh, it leads to a positive contribution into $\mathrm{Im}(\omega)$ from the first term on the RHS of the ω-equation which approximately compensates the upwind contribution coming from the second term on the RHS. The compensation does not occur at small scales, and they are damped with the upwind diffusion.

Returning to the choice of the stabilization parameter ε_t suggested in Section 4 we could mention that in most cases it is determined by the time step Δt, as accuracy consideration require it to be smaller than $h/|u|$. Thus we always have $\bar{\varepsilon}_t < 0.5$. However stabilization could only be efficient at small scales if $\bar{\varepsilon}_t$ exceeds Pe^{-1}, and some adjustment of ε_t might be necessary if it turns to be too small due to the time step used.

Appendix B. Barotropic–baroclinic splitting

Splitting of the problem (15) and (16) into barotropic and baroclinic parts requires special approach in the case of 3D FE discretization employed here. Since the vertically integrated momentum equation should be consistent with (15), it could only be obtained by choosing a special subspace of the test functions $\tilde{\mathbf{u}}(\lambda, \theta, z) = \tilde{\mathbf{u}}(\lambda, \theta)$. Consider, for example, the Coriolis term in the momentum equation (15). It becomes

$$\int_\Omega f\mathbf{k} \times \mathbf{u}\tilde{\mathbf{u}}(\lambda,\theta)\,\mathrm{d}\Omega = \int_{\Gamma_1} f\mathbf{k} \times \left(\int \mathbf{u}\,\mathrm{d}z\right)\tilde{\mathbf{u}}(\lambda,\theta)\,\mathrm{d}\Gamma_1 = \int_{\Gamma_1} f\mathbf{k} \times \mathbf{U}\tilde{\mathbf{u}}(\lambda,\theta)\,\mathrm{d}\Gamma_1,$$

with $\mathbf{U} = \int \mathbf{u}\,\mathrm{d}z$ the horizontal transport. Here Γ_1 stands for the ocean surface. Clearly $\mathbf{U}$ does not belong to the space of linear functions on surface triangles if $\mathbf{u}$ is linear on tetrahedra. For that

reason, the "strong-sense" definition $\mathbf{U} = \int \mathbf{u}\,\mathrm{d}z$ is not allowed and we have to adopt the "weak-sense" definition

$$\int_{\Gamma_1} \mathbf{U}\tilde{\mathbf{u}}(\lambda,\theta)\,\mathrm{d}\Gamma_1 = \int_{\Omega} \mathbf{u}\tilde{\mathbf{u}}(\lambda,\theta)\,\mathrm{d}\Omega,$$

equivalent to $2N_{2D}$ equations to determine nodal values of transport $\mathbf{U}$ by known 3D nodal values of $\mathbf{u}$.

The time derivative could be treated in the same way, while viscous terms are written as $\int_{\Gamma_1} A_l \nabla\mathbf{U}\nabla\tilde{\mathbf{u}}\,\mathrm{d}\Gamma_1$ on the LHS, with the difference between the actual vertically integrated dissipation and the latter term $D = \int_{\Gamma_1}(A_l(\int \nabla\mathbf{u}\,\mathrm{d}z - \nabla\mathbf{U})\nabla\tilde{\mathbf{u}})\,\mathrm{d}\Gamma_1$, accounted for in the RHS. With such definitions and rearrangements, the 2D equations that follow could be solved for $\mathbf{U}_k$, ζ_k at each time step. The transport obtained cannot be used directly, and we could either substitute ζ and solve for $\mathbf{u}$ at 3D nodes, or find baroclinic velocities $\mathbf{u}_{bc}$ at 3D nodes and solve for a 2D barotropic correction field $\mathbf{u}_{bt}(\lambda,\theta)$ the system of equations $\int_{\Omega}(\mathbf{u}_{bc} + \mathbf{u}_{bt})\tilde{\mathbf{u}}(\lambda,\theta)\,\mathrm{d}\Omega = \int_{\Gamma_1} \mathbf{U}\tilde{\mathbf{u}}(\lambda,\theta)\,\mathrm{d}\Gamma_1$. Whatever the approach used, the problem arises with the term D introduced above. It turns to be too noisy, and degrades the quality of the solution. This is the main reason explaining why we currently solve the combined system of equations (15) and (16) for the full horizontal velocity $\mathbf{u}$ and sea surface height ζ. Further work is needed to implement splitting.

References

Babuška, I., 1973. The finite element method with Lagrangian multipliers. Numer. Math. 20, 179–192.

Brasseur, P.P., 1991. A variational inverse method for the reconstruction of general circulation fields in the Northern Bering Sea. J. Geophys. Res. 96C, 4891–4907.

Brezzi, F., 1974. On the existence, uniqueness and approximation of saddlepoint problems arising from Lagrangian multipliers. R.A.I.R.O. Anal. Numer. R2, 129–151.

Brezzi, F., Marini, D., Russo, A., 1996. Pseudo residual–free bubbles and stabilized methods. In: Désideri, J.A. et al. (Eds.), Computational Methods in Applied Sciences. John Wiley and Sons Inc., pp. 3–8.

Bryan, K., Manabe, S., Pacanowski, R.C., 1975. A global ocean-atmosphere climate model. Part II: The oceanic circulation. J. Phys. Oceanogr. 5, 30–46.

Codina, R., Soto, O., 1997. Finite element solution of the Stokes problem with dominating Coriolis force. Comput. Meth. Appl. Mech. Engng. 142, 215–234.

Chassignet, E.P., Arango, H., Dietrich, D., Ezder, T., Ghil, M., Haidvogel, D.B., Ma, C.-C., Mehra, A., Paiva, A.M., Sirkes, Z., 2000. DAMÉE-NAB: the base experiment. Dyn. Atmos. Oceans 32, 155–183.

Deleersnijder, E., 2001. Enforcing the continuity equation in numerical models of geophysical fluid flows. Appl. Math. Lett. 14, 867–873.

Dobrindt, U., Frickenhaus, S., 2000. Partitioning, reordering and solving an advection–diffusion problem formulated in finite elements. Alfred Wegener Institute for Polar and Marine Research, Berichte aus dem Fachbereich Physik, Report 98.

Dobrindt, U., Schröter, J., 2002a. An adjoint ocean model using finite elements: an application to the South Atlantic. J. Atm. Oceanic Technol., in press.

Dobrindt, U., Schröter, J., 2002b. A finite element inverse ocean model for an advection–diffusion problem. Comput. Meth. Appl. Mech. Engng., in press.

Dumas, E., Provost, C., Poncet, A., 1982. Feasibility of finite element methods for oceanic general circulation modelling. In: 4th International Conference on Finite Element in Water Resources. Springer-Verlag, New York, pp. 43–55.

Fix, G.J., 1975. Finite element model for ocean circulation problems. SIAM J. Appl. Math. 29, 371–387.

Franca, L.P., Russo, A., 1996. Approximation of the Stokes problem by residual-free macro bubbles. East-West J. Appl. Math 4, 265–278.

Gerdes, R., Köberle, C., Willebrand, J., 1991. The influence of numerical advection schemes on the results of ocean general circulation models. Climate Dyn. 5, 211–226.

Griffies, S.M., Böning, Bryan, F.O., Chassignet, E.P., Gerdes, R., Hasumi, H., Hirst, A., Treguier, A.-M., Webb, D., 2001. Developments in ocean climate modelling. Ocean Modell. 2, 123–192.

Haidvogel, D.B., Arango, H.G., Hedstrom, K., Beckmann, A., Malanotte-Rizzoli, P., Shchepetkin, A.F., 2000. Model evaluation experiments in the North Atlantic Basin: simulations in nonlinear terrain-following coordinates. Dyn. Atmos. Oceans 32, 239–281.

Hanert, E., Legat, V., Deleersnijder, E., 2003. A comparison of three finite elements to solve the linear shallow water equations. Ocean Modell. 5, 17–35.

Hecht, M.W., Wingate, B.A., Kassis, P., 2000. A better, more discriminating problem for ocean tracer transport. Ocean Modell. 2, 1–5.

Hughes, T.J.R., Franca, L.P., Hubert, G.M., 1989. A new finite element formulation for computational fluid dynamics: VIII. The Galerkin-least-squares method for advective–diffusive equations. Comput. Meth. Appl. Mech. Engng. 73, 173–189.

Hughes, T.J.R., 1995. Multiscale phenomena: Green's functions, the Dirichlet-to-Neumann formulation, subgrid scale models, bubbles and the origins of stabilized methods. Comput. Meth. Appl. Mech. Engng. 127, 387–401.

Iakovlev, N.G., 1996. A numerical model and preliminary results of calculations to reproduce the summer circulation in the Kara Sea. Izvestiya Atmos. Oceanic Phys. 32, 660–668 (Translated from Izvestiya AN, Fizika Atmosfery i Okeana).

Ilinka, F., Hétu, J.-F., Pelletier, D., 2000. On stabilized finite element formulation for incompressible advective–diffusive transport and fluid flow problems. Comput. Meth. Appl. Mech. Engng. 188, 235–255.

Iskandarani, M., Haidvogel, D.B., Boyd, J.P., 1995. A staggered spectral model with application to the oceanic shallow water equations. Int. J. Numer. Meth. Fluids 20, 393–414.

Karypis, G., Kumar, V., 1997. Parallel Threshold-based ILU Factorization. Technical Report 96-061, University of Minnesota, Department of Computer Science/Army HPC Research Center Minneapolis, MN 55455.

Karypis, G., Kumar, V., 1998. METIS-a software package for partinioning unstructured graphs, partitioning meshes and computing fill—reducing ordering of sparse matrices, version 4.0. University of Minnesota, Department of Computer Science/Army HPC research Center, Minneapolis.

Ladyzhenskaya, O.A., Solonnikov, V.A., 1976. On some problems in vector analysis and weak formulations of boundary value problems for the Navier–Stokes equations. Zapiski nauchnykh seminarov LOMI, Leningrad 69, 81–118 (in Russian).

Le Provost, C., 1986. On the use of finite element methods for ocean modelling. In: O'Brien, J.J. (Ed.), Advanced Physical Oceanographic Numerical Modelling, D. Reidel Publishing, pp. 557–580.

Le Provost, C., Vincent, P., 1991. Finite element for modelling ocean tides. In: Parker, B. (Ed.), Tidal Hydrodynamics. John Wiley, New York, pp. 41–60.

Le Roux, D.Y., Staniforth, A., Lin, C.A., 1998. Finite elelments for shallow water equation ocean model. Mon. Weather Rev. 126, 1931–1951.

Levin, J.G., Iskandarani, M., Haidvogel, D.B., 1997. A spectral filtering procedure for eddy-resolving simulations with a spectral element model. J. Comput. Phys. 137, 130–154.

Lynch, D.R., Naimie, C.E., 1993. The M_2 tide and its residual on the outer banks of the Gulf of Maine. J. Phys. Ocenogr. 23, 2222–2253.

Lynch, D.R., Ip, J.T.C., Naimie, C.E., Werner, F.E., 1996. Comprehensive coastal circulation model with application to the Gulf of Maine. Cont. Shelf Res. 16, 875–906.

Muccino, J.C., Gray, W.G., Foreman, G.G., 1997. Calculation of vertical velocity in three-dimensional, shallow water equation, finite element models. Int. J. Numer. Meth. Fluids 25, 779–802.

Myers, P.G., Weaver, A.J., 1995. A diagnostic barotropic finite-element ocean circulation model. J. Atm. Oceanic Technol. 12, 511–526.

Marchesiello, P., McWilliams, J.C., Shchepetkin, A., 2001. Open ocean boundary conditions for long-term integration of regional oceanic models. Ocean Modell. 3, 1–20.

Nechaev, D., Schröter, J., Yaremchuk, M., 2003. A diagnostic stabilized finite-element ocean circulation model. Ocean Modell. 5, 37–63.

Patera, A.T., 1984. A spectral element method for fluid dynamics: Laminar flow in a channel expansion. J. Comput. Phys. 54, 468–488.

Pacanowski, R.C., Griffies, S.M., 2000. MOM 3.0 Manual. Available from http://www.gfdl.gov/~smg/MOM/web/guide_parent/guide_parent.html.

Schlichtholz, P., Houssais, M.-N., 1999. An inverse modelling study in Fram Strait. Part I: dynamics and circulation. Deep-Sea Res. II 46, 1083–1135.

Trenberth, K., Olson, J., Large, W., 1989. A global ocean wind stress climatology based on ECMWF analyses. Technical Report NCAR/TN-338+STR, National Center for Atmospheric Research, Boulder, Colorado.

Walters, R.A., Werner, F.E., 1989. A comparison of two finite-element models of tidal hydrodynamics using a North Sea data set. Adv. Water Resour. 12, 184–193.

Webb, D.J., de Cuevas, B.A., Richmond, C.S., 1998. Improved advection schemes for ocean models. J. Atmos. Ocean. Tech. 15, 1171–1187.

Westerink, J.J., Luettich, R.A., Blain, C.A., Scheffner, N.W., 1992. ADCIRC: An Advanced Three-Dimensional Circulation Model for Shelves, Coasts and Estuaries; Report 2: Users Manual for ADCIRC-2DDI. Contractors Report to the US Army Corps of Engineers, Washington, DC, July 1992.

Wunsch, C., Haidvogel, D.B., Iskandarani, M., 1997. Dynamics of the long-period tides. Prog. Oceanogr. 40, 81–108.